High-frequency ultrasound backscattering by blood: Analytical and semianalytical models of the erythrocyte cross section

David Savéry[a] and Guy Cloutier[b]
Laboratory of Biorheology and Medical Ultrasonics, University of Montreal Hospital Research Center, 2099 Alexandre de Séve, Room Y-1619-Pavillion de Séve, Notre-Dame Hospital, Montréal, Québec H2L 2W5, Canada

(Received 27 July 2006; revised 13 February 2007; accepted 15 February 2007)

This paper proposes analytical and semianalytical models of the ultrasonic backscattering cross section (BCS) of various geometrical shapes mimicking a red blood cell (RBC) for frequencies varying from 0 to 90 MHz. By assuming the first-order Born approximation and by modeling the shape of a RBC by a realistic biconcave volume, different scattering behaviors were identified for increasing frequencies. For frequencies below 18 MHz, a RBC can be considered a Rayleigh scatterer. For frequencies less than 39 MHz, the general concept of acoustic inertia tensor is introduced to describe the variation of the BCS with the frequency and the incidence direction. For frequencies below 90 MHz, ultrasound backscattering by a RBC is equivalent to backscattering by a cylinder of height 2 μm and diameter 7.8 μm. These results lay the basis of ultrasonic characterization of RBC aggregation by proposing a method that distinguishes the contribution of the individual RBC acoustical characteristics from collective effects, on the global blood backscattering coefficient. A new method of data reduction that models the frequency dependence of the ultrasonic BCS of micron-sized weak scatterers is also proposed. Applications of this method are in tissue characterization as well as in hematology. © *2007 Acoustical Society of America.* [DOI: 10.1121/1.2715452]

PACS number(s): 43.80.Qf, 43.80.Ev, 43.20.Bi, 43.20.Fn [FD] Pages: 3963–3971

I. INTRODUCTION

A. Background

Ultrasound (US) tissue characterization techniques provide means to assess the pathophysiological state of organs by measuring a number of ultrasonic tissue properties. There is however a certain need to understand how these measurable acoustical indices relate to biophysical phenomena occurring at the cellular or the subcellular scale. Tissue microstructural characteristics (such as cell size, cellular organization, fiber anisotropy, etc.) are indeed expected to provide meaningful information for diagnosis, as they are directly related to biological processes.

Previous works in ultrasonic tissue characterization have studied the relation between the microstructure and various acoustical tissue properties as the backscattering coefficient and spectral characteristics.[1,2] The typical approach considers that mammal tissue can be acoustically modeled as a continuous random distribution of mass density and bulk compressibility. The correlation length of their correlation function can be related to the size of a discrete microscopic scatterer, with replicas randomly spread in the bulk volume. The propagation of the interrogating US wave within this type of medium is conditioned by the particle acoustic properties, the properties of the embedding medium, the particle number density and size, and the level of spatial organization of the scatterers.

This paper focuses on a typical example of heterogeneous biological milieu: blood. This biofluid can be mechanically described as a colloidal suspension of flexible cells flowing within the plasma, which is itself a Newtonian liquid. Erythrocytes form the vast majority of blood cells (99% in number) and occupy a large volume fraction (hematocrit) of 35–45% under normal conditions. Because of the coexistence of erythrocytes and liquid phases, blood exhibits a shear-thinning rheological behavior. When flowing at a low shear rate, red blood cells (RBCs) adhere and form a structured network of clusters. The increase of the shear rate results in a reversible disaggregation of RBCs. The intricate packing of the so-called *rouleaux* of RBCs results in a viscosity increase. In various pathological conditions, including cardiovascular diseases and hemoglobinopathies, blood viscosity is abnormally high. Hemodynamics can be markedly affected by such hyperviscosity syndrome, especially in the microcirculation.

Several groups are investigating the possibility to detect abnormal RBC aggregation and the associated hemorheological disorders with US. Some clinical observations of blood hyperechogenicity appearing in low shear or static flow conditions have qualitatively demonstrated the potential of US to image RBC aggregation. This phenomenon is encountered in echocardiography or in vascular imaging and was given the name of spontaneous echo contrasts or smoke-like echoes.[3,4] A better quantification of this scattering enhancement would allow the extraction of valuable biophysical parameters that characterize red cell adhesion.

The measurement of RBC aggregation indices (aggregate size, anisotropy, etc.) through the quantification of blood

[a]Present address: Supersonic Imagine, Aix-en-Provence, France.
[b]Electronic mail: guy.cloutier@umontreal.ca

ultrasound backscattering however requires an acoustical model. Before understanding backscattering of US by an ensemble of interacting RBCs, a first obvious step is to properly quantify US backscattering by a single erythrocyte. This is the purpose of this paper.

B. Literature review

At a low frequency (in the range of a few megahertz) and for weak scattering particles, the relation between the backscattering cross section (BCS) and the RBC acoustical properties is simple and is conveyed by the Rayleigh formulation.[5] In this approximation, subwavelength geometric details do not affect the BCS and therefore cannot be inferred by "inverting" low frequency scattering data. In the case of red blood cells, the validity of the Rayleigh assumption can be questioned when the acoustical frequency exceeds 27 MHz. This approximation is indeed valid when $ka \ll 1$, where $k=\omega/c$ is the wave number and $a=2.82$ μm is the effective erythrocyte radius. The effective radius is defined in this paper as $4\pi a^3/3=V_s$ where V_s is the volume of the RBC, roughly 94 μm^3. When the frequency is above 27 MHz, $ka=\pi/10\approx 0.31$ considering that the speed of sound $c=1540$ m/s (Ref. 6) and therefore the Rayleigh validity is questionable. As high frequency ultrasound imaging systems (intravascular imaging, small animal scanners) currently use frequencies above 20 MHz, the need to extend Rayleigh formulation of the BCS seems obvious.

A few studies of various domains of acoustics experimentally, theoretically or numerically examined non-Rayleigh aspects of weak acoustical backscattering when ka becomes nonnegligible. In marine acoustics, Stanton *et al.*[7] proposed a number of models of the angle-averaged backscattering cross section of individual zooplankton based on the Born first-order approximation. By modeling the animals as bent cylinders for $ka \leqslant 5$, the study showed good agreements between predictions given by the backscattering models (obtained by measuring animal dimensions) and experimental acoustical data. This proved the utility of the simple first-order Born approximation to take into account the complex geometry of the scatterer.

For the problem of ultrasound backscattering by a single red blood cell, Kuo and Shung[8] and Coussios[9] also discussed the limitations of the Rayleigh formulation. Kuo and Shung[8] measured the backscattering coefficient of a diluted suspension of porcine RBCs and the experimentally determined BCS was shown to scale as $k^4V_s^2$ for frequencies below 30 MHz, as predicted by the Rayleigh approximation. In the same study, numerical results obtained by the Jakeman's T-matrix method predicted that the red cell shape affected the BCS and that the frequency dependence only slightly deviated from $k^4V_s^2$ for $ka<1$ (87 MHz). This study considered frequencies from 1 MHz to 1.7 GHz, approximately. Coussios[9] analytically derived the BCS of a thin cylinder with approximate RBC dimensions, using the Born weak scattering assumption and showed that the spherical and cylinder models gave similar values of the BCS for frequencies $\leqslant$20 MHz. The effect of the particle shape became only significant for frequencies above 20 MHz (the maximum frequency considered in this study being 60 MHz).

C. Objectives

Following these studies, this paper has two objectives. The analytical framework opened by Coussios[9] who used the Born approximation is generalized to take into account the realistic biconcave shape of the RBC. Analytical or semi-analytical results are then used to predict how microscale geometric features influence the high frequency BCS of erythrocytes above 20 MHz. It is shown that different scattering behaviors can be distinguished depending on the ultrasonic frequency.

II. THEORY AND METHODS

A. The backscattering cross section

The ability of a material particle to generate acoustical echoes is commonly quantified by the BCS that is defined as follows. Consider a monochromatic plane wave with complex amplitude $p_i(\mathbf{r})=p_0e^{i\mathbf{k}\cdot\mathbf{r}}$, where $\mathbf{r}$ is the spatial vector, p_0 is the incident pressure amplitude, and $\mathbf{k}$ represents the wave vector. This pressure wave propagates in a linear fluid characterized by a mass density ρ_0 and an adiabatic compressibility κ_0. A fluid particle of volume V_s centered in O creates a fluctuation of density and compressibility. The interaction between the incident wave and the particle results in a deviation of the incident wave that redistributes the acoustical energy in space.[10] The total pressure amplitude $p(\mathbf{r})$ can be mathematically decomposed as the sum of the unperturbated incident pressure field $p_i(\mathbf{r})$ and of the scattered pressure $p_s(\mathbf{r})$. In the far field of the particle, the scattered field has the asymptotic form[11]

$$p_s(r\mathbf{e}_r)=p_0\frac{e^{i\mathbf{k}\cdot\mathbf{r}+i\theta_0}}{r}\sigma(\mathbf{e}_r,\mathbf{k})^{1/2}. \tag{1}$$

In this expression, $\mathbf{e}_r$ is the unit vector pointing in the observation direction, θ_0 is a phase term (that will not be further discussed in this paper), and $\sigma(\mathbf{e}_r,\mathbf{k})$ is the scattering cross section of the particle. In pulse-echo US, when the target lies in the far field of the transducer, the scattering direction that mainly contributes to the transduced radio-frequency signal corresponds to the reverse direction: $\mathbf{e}_r=-\mathbf{k}/k$. For this reason, the quantity that characterizes particle backscattering is the backscattering cross-section (noted σ_b) defined as $\sigma_b(\mathbf{k})=\sigma(-\mathbf{k}/k,\mathbf{k})$.

In the rest of the paper, one will be interested only in backscattering, and therefore the term insonification angle or simply angle will be used to describe the direction of the wave vector $\mathbf{k}$ with respect to the RBC. There will be no ambiguity on the scattering vector direction which is simply $-\mathbf{k}$.

B. Rayleigh scattering

The expression of the BCS of a small fluid sphere ($ka \ll 1$) that has a constant density $\rho=\rho_0(1+\gamma_\rho)$ and compressibility $\kappa=\kappa_0(1+\gamma_\kappa)$, where γ_ρ and γ_κ are the relative con-

trasts in density and compressibility with respect to the background medium, was originally derived by Rayleigh (see Ref. 10). It can be expressed as

$$\sigma_b(\mathbf{k}) = \frac{k^4 V_s^2}{16\pi^2}\left(\gamma_\kappa - \frac{\gamma_\rho}{1-\gamma_\rho/3}\right)^2. \quad (2)$$

In the case of a weak scatterer, the contrast values γ_ρ and γ_κ are small and a second-order approximation reduces Eq. (2) to:

$$\sigma_b(\mathbf{k}) = \frac{k^4 V_s^2}{4\pi^2}\gamma_z^2, \quad (3)$$

where $\gamma_z = (\gamma_\rho - \gamma_\kappa)/2$ is the small relative contrast of acoustical impedance between the scatterer and the surrounding medium. It can be noted that the acoustic cross section of a small sphere scales as the fourth power of frequency and therefore increases rapidly with increasing frequency.

C. Form factor of a homogeneous scatterer considering the Born approximation

Equation (3) is valid for a small, homogeneous, and weak spherical scatterer. Now, for any type of scattering particle, a nondimensional corrective term $F(\mathbf{k})$, named the form factor, can be defined as

$$\sigma_b(\mathbf{k}) = \frac{k^4 V_s^2}{4\pi^2}\langle\gamma_z\rangle^2 F(\mathbf{k}), \quad (4)$$

where $\langle\gamma_z\rangle = (1/V_s)\int_{V_s}\gamma_z(r)d^3r$ represents the spatially averaged impedance contrast of the particle. The deviation of the form factor from one quantifies the influence of the particle geometry and orientation on the BCS. In the Born approximation ($p_s \ll p_i$) that applies for weak scattering conditions, the form factor has a simple expression [easily retrieved from Eq. (8.1.20) of Ref. 10] related to the spatial Fourier spectrum of the impedance contrast:

$$F(\mathbf{k}) = \frac{1}{\langle\gamma_z\rangle^2 V_s^2}\left|\int_{V_s}\gamma_z(r)e^{2i\mathbf{k}\cdot\mathbf{r}}d^3r\right|^2. \quad (5)$$

This expression is in agreement with the fact that the form factor approaches unity (and Rayleigh scattering) when the particle size is negligible with respect to the wavelength ($e^{2i\mathbf{k}\cdot\mathbf{r}} \to 1$).

D. Form factors of simple geometrical shapes

Analytical expressions of the form factor can be found for homogeneous scatterers having simple shapes. The case of three important shapes (sphere, ellipsoid, and cylinder) is given in Table I. The range of wave numbers for which Rayleigh scattering applies within 5% accuracy is also indicated. Note that these analytical forms are compatible with Ref. 12 for spheres and ellipsoids and the cylinder form agrees with the general expression obtained by Coussios [Eq. (13) of Ref. 9].

TABLE I. Form factors of several descriptive shapes. The wave vector $\mathbf{k}$ is decomposed in the ellipsoid system of axes $\mathbf{k}=k_1\mathbf{e}_1+k_2\mathbf{e}_2+k_3\mathbf{e}_3$, where (1, 2, and 3 or x, y, and z) refer to the ellipsoid principal directions of the axes (a_1, a_2, and a_3), or in a cylindrical system of axes $\mathbf{k}=k_z\mathbf{e}_z+k_r\mathbf{e}_r$. The height of the cylinder is h_0 and its radius is R. The form factor of the sphere is $F(\mathbf{k})=\Phi_s(2ka)$, where a is its radius. J_1 is the first-order Bessel function.

Particle shape	Form factor $F(\mathbf{k})$	Rayleigh limit $[F(\mathbf{k})>0.95]$
Sphere	$\Phi_s(2ka)$, $\Phi_s(u)=(3\sin u-3u\cos u)^2/u^6$	$ka<0.25$
Ellipsoid	$\Phi_s(2((k_1a_1)^2+(k_2a_2)^2+(k_3a_3)^2)^{1/2})$	$((k_1a_1)^2+(k_2a_2)^2+(k_3a_3)^2)^{1/2}<0.25$
Cylinder	$(\sin k_zh_0/k_zh_0)^2\times(J_1(2k_rR)/k_rR)^2$	$(k_z^2h_0^2+3k_r^2R^2)^{1/2}<0.38$

E. Form factor of an axisymmetrical particle mimicking a RBC

Consider now a homogeneous particle having the symmetries of a RBC (see Fig. 1), i.e., a symmetry of revolution around (O_z) and a mirror symmetry with respect to (O_{xy}). The shape of the RBC can then be described by the radial profile:[13]

$$z_0(r) = \frac{h_0}{2}\phi(2r/D), \quad (6)$$

where h_0 is the particle thickness along (O_z), $\phi(u)$ is the normalized geometric profile, and D is the diameter. This function, defined for $u\in[0,1]$, describes the particle shape and satisfies $\phi(0)=1$, $\phi(1)=0$. As detailed in Appendix A, the form factor of the RBC can be formulated by using Eq. (3) and by considering that the acoustic impedance is constant, i.e., $\gamma_z(\mathbf{r})=\langle\gamma_z\rangle$ when $\mathbf{r}$ lies within the RBC and $\gamma_z(\mathbf{r})=0$ when $\mathbf{r}$ is outside of the RBC. This yields to

$$F(k_r\mathbf{e}_r,k_z\mathbf{e}_z) = \left|\int_0^1 u\phi(u)J_0(k_rDu)\frac{\sin(k_zh_0\phi(u))}{k_zh_0\phi(u)} \times du \Big/ \int_0^1 u\phi(u)du\right|^2, \quad (7)$$

where J_0 is the Bessel function of order 0.

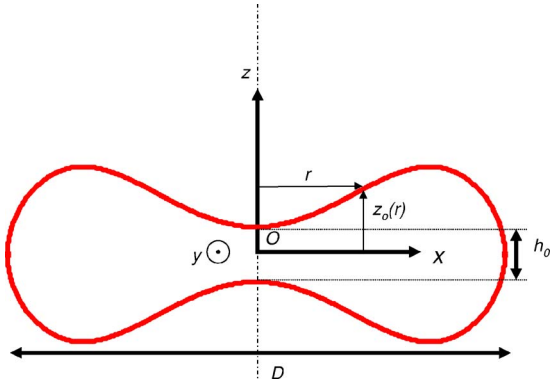

FIG. 1. (Color online) Geometric cross section of a red blood cell defined by the function $z_0(r)$, where h_0 is the thickness along O_z and D is the diameter along O_{xy}.

F. Acoustical inertia tensor

A second order expansion of $F(\mathbf{k})$ in ka is helpful to examine the deviation of the form factor of a homogeneous particle from one when the frequency is increased. As detailed in Appendix B, a second order Taylor expansion of Eq. (A1) gives:

$$F(\mathbf{k}) = 1 - 4\mathbf{k}\cdot\boldsymbol{\Sigma}\mathbf{k} + o(k^2a^2), \tag{8}$$

where $\boldsymbol{\Sigma}$ is a second order symmetrical positive tensor, a characteristic tensor of the particle shape referred here as the acoustical inertia tensor, defined by

$$\boldsymbol{\Sigma} = \frac{1}{V_s}\int_{V_s} \mathbf{r}\otimes\mathbf{r}d^3r. \tag{9}$$

In Eq. (9), the dyadic product of the two vectors is noted $\otimes$. The principal axes of the particle are the eigenvectors of $\boldsymbol{\Sigma}$ and its eigenvalues noted $\boldsymbol{\Sigma}_{11}\leqslant\boldsymbol{\Sigma}_{22}\leqslant\boldsymbol{\Sigma}_{33}$ scale as the surface of the particle. Note that the acoustical inertia tensor $\boldsymbol{\Sigma}$ as defined here is directly related to the inertia tensor $\mathbf{J}$ (as defined in solid mechanics) of a solid particle of unit mass density rotating around $\mathbf{O}$ (part 5.3.1 of Ref. 14):

$$\mathbf{J} = \mathrm{tr}(\boldsymbol{\Sigma})\mathbf{U} - \boldsymbol{\Sigma}, \tag{10}$$

where $\mathbf{U}$ is the identity tensor and tr represents the trace. This analogy leads us to name this tensor *acoustical inertia tensor*, as it directly relates to the inertia moments of a rigid particle having the same shape. To give an example, an ellipsoid of semi-axes $\{a_i\mathbf{e}_i\}_{i=1,2,3}$ has an acoustical inertia tensor $\boldsymbol{\Sigma}$ of expression:

$$\boldsymbol{\Sigma} = \frac{a_1^2}{5}\mathbf{e}_1\otimes\mathbf{e}_1 + \frac{a_2^2}{5}\mathbf{e}_2\otimes\mathbf{e}_2 + \frac{a_3^2}{5}\mathbf{e}_3\otimes\mathbf{e}_3. \tag{11}$$

For the case of the symmetrical particles as described earlier in Eq. (6), the inertia tensor is diagonal in the base $\{\mathbf{e}_x,\mathbf{e}_y,\mathbf{e}_z\}$ and can be expressed as:

$$\boldsymbol{\Sigma} = \left(D^2\frac{\int_0^1 u^3\phi(u)du}{8\int_0^1 u\phi(u)du}(\mathbf{e}_x\otimes\mathbf{e}_x + \mathbf{e}_y\otimes\mathbf{e}_y) + h_0^2\frac{\int_0^1 u\phi(u)^3du}{12\int_0^1 u\phi(u)du}\mathbf{e}_z\otimes\mathbf{e}_z \right). \tag{12}$$

This reduces to $\boldsymbol{\Sigma} = D^2/16(\mathbf{e}_x\otimes\mathbf{e}_x + \mathbf{e}_y\otimes\mathbf{e}_y) + h_0^2/12\mathbf{e}_z\otimes\mathbf{e}_z$ in the case of a cylinder of diameter D and height h_0 ($\phi(u) = 1$ for $|u|<1$).

G. Modeling of the physical and geometrical properties of plasma and of a erythrocyte

In this study, the plasma is supposed non-viscous, characterized by a compressibility $\kappa_p = 4.09\times10^{-10}$ Pa^{-1} and a mass density $\rho_p = 1021$ kg m^{-3} (see Ref. 15). The hemoglobin solution encapsulated by the RBC membrane is supposed nonviscous and acoustically described by the compressibility $\kappa_{\mathrm{RBC}} = 3.41\times10^{-10}$ Pa^{-1} and mass density $\rho_{\mathrm{RBC}} = 1092$ kg m^{-3}. The resulting impedance contrast defined in Eq. (3) is $\gamma_z = 0.13$. The effect of the RBC membrane on acoustical scattering is neglected. This assumption is based on the fact that the membrane of an intact RBC has a small thickness of 10 nm. It could be argued that the measured backscattering by ghost cells (damaged red cells with removed hemoglobin) is far from negligible (see Ref. 16, Chap. 7) and this could be attributed to membrane backscattering effects. However, as carefully discussed in Ref. 16, this interpretation seems inappropriate. Membranes of damaged cells act like nets, which suggest that lysed cells are actually smaller but denser particles that strongly scatter US.

Red cells are very deformable and their shapes vary in response to mechanical stress (e.g., the hemodynamic shear forces) and to the osmolarity of the surrounding environment. In static equilibrium, as shown in Fig. 1, the RBC is a biconcave disk[13] with a volume $V_s = 4\pi a^3/3 = 94$ μm^3 (effective radius $a = 2.82$ μm) and an optimal exchange surface area of 135 μm^2. The mean axial and radial maximum dimensions are, respectively, $h_0 = 0.81$ μm and $D = 7.82$ μm. Evans and Fung[13] have formulated a convenient analytic formula that gives the normalized profile of a nonstressed RBC membrane:

$$\phi(u) = \sqrt{1-u^2}(1 + \alpha_2u^2 + \alpha_4u^4), \tag{13}$$

where $\alpha_2 = 9.7$ and $\alpha_4 = -5.4$.

H. Backscattering cross sections of particles mimicking a RBC

According to Eq. (4) and knowing the values of V_s and γ_z, one can derive the backscattering cross-section of elementary particles from the definition of the form factor $F(\mathbf{k})$. Table I provides analytical expressions of $F(\mathbf{k})$ for a sphere, an ellipsoid and a cylinder. By considering cylindrical coordinates, the form factor of a biconcave disk that better mimic the shape of a RBC was shown in Eq. (7). Numerical integration is required to compute this form factor. Equations (8) and (12) can also be utilized if one uses Cartesian coordinates.

At the second order in ka and if the Born approximation holds, the frequency dependence of the red cell BCS is given by a Taylor expansion using Eq. (4) and the definition of the inertia axes introduced earlier in Sec. II F [Eqs. (8) and (11)]. This results in

$$\sigma_b(\mathbf{k}) = \frac{k^4V_s^2}{4\pi^2}\gamma_z^2\left(1 - \frac{4}{5}k_x^2a_x^2 - \frac{4}{5}k_y^2a_y^2 - \frac{4}{5}k_z^2a_z^2\right) + o(k^6). \tag{14}$$

Two particles with the same material properties but different shapes will have equivalent backscattering behaviors (up to the sixth order in ka and for all insonification angles) if they have the same volume and the same inertia axes.

TABLE II. Volume V and inertia characteristics of the red blood cell and other equivalent descriptive shapes. The equivalent axes a_i are computed from the eigenvalues $a_i^2/5$ of the inertia tensor $\mathbf{\Sigma}$. The geometrical descriptors h_0, D, and a are, respectively, the height, the diameter, and the effective radius of the red blood cell (a is the radius of the sphere with equivalent volume).

Particle shape	Volume (μm^3)	Inertia axes $a_x/a=a_y/a$	Inertia axis a_z/a	Geometrical descriptors (μm)
Red blood cell	94	1.54	0.50	$h_o=0.81$ $D=7.82$
Sphere	94	1	1	$a=2.82$
Ellipsoid	94	1.54	0.42	$a_z=V/(4\pi a_x^2/3)$
Cylinder	94	1.54	0.46	$h_o=V/(\pi D^2/4)=2$ $D=2\sqrt{0.8}a_x=7.76$

I. Numerical integration

The different definite integrals involved to compute the form factors were computed by a trapezoidal method. The interval $[0, 1]$ was divided in $N=10^4$ segments.

III. RESULTS

A. Dimensions of the equivalent particles

The inertia axes of the model of a red cell were computed using Eqs. (11) and (12). Adjunct to the volume, these quantities allow to derive the dimensions of the equivalent sphere (same volume), of the equivalent ellipsoid (same volume and same radial inertia axes) and of the equivalent cylinder (same volume and same radial inertia axes) as given in Table II. Cross sections of these different shapes are represented in Fig. 2 for visual comparison.

B. Form factor of the particles

The variations of the various form factors as a function of the frequency and two different angles are given in Fig. 3. The decrease of the form factor from one to zero depends on the scattering shape and on the direction of insonification. The more elongated a particle is along the incident direction, the faster the form factor decreases as a function of frequency. In other words, the backscattering as a function of the incidence angle is maximal when the propagation direction is aligned with the smallest inertia axis ($k=k_z$). The incident wave perpendicularly intersects the biggest section of the particles.

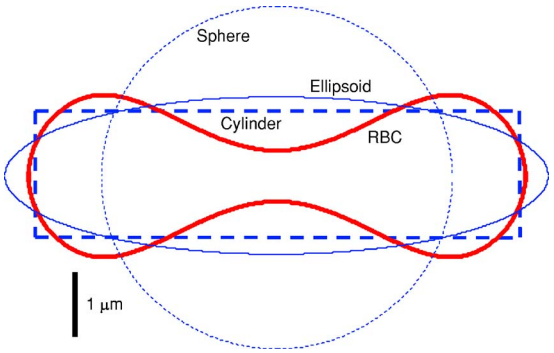

FIG. 2. (Color online) Geometric cross sections of a red blood cell and equivalent descriptive shapes.

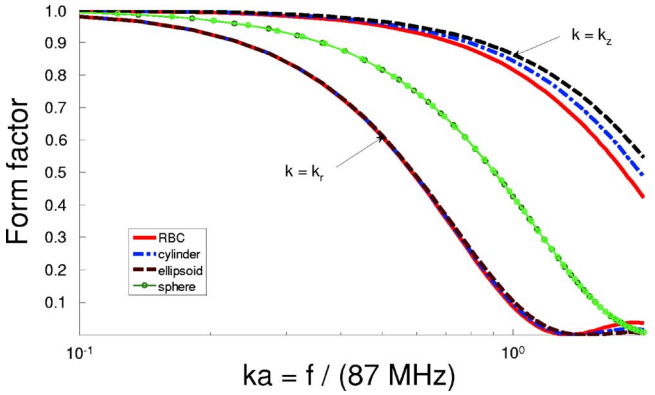

FIG. 3. (Color online) Variation of the form factor as a function of the reduced size parameter (ka) for different descriptive shapes. The insonification direction is either along O_z ($k=k_z$) or perpendicular to it ($k=k_r$).

C. Frequency dependence of the backscattering cross-section

Figure 4 shows the backscattering cross section of a RBC and of the equivalent simpler shapes along the O_z and O_x axes, as a function of ka. Along O_z, with the exception of the spherical descriptor, the backscattering behavior only slightly deviates from Rayleigh scattering below 87 MHz. Perpendicular to the long axis of each particle, non-Rayleigh behavior quickly arises for all shape descriptors as the frequency is increased.

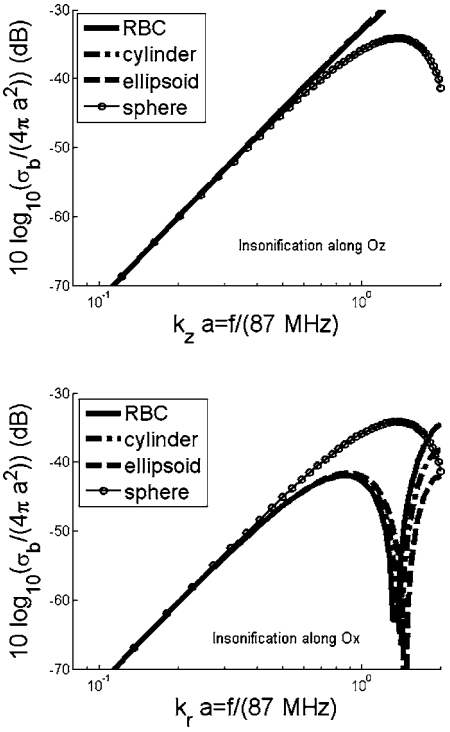

FIG. 4. Normalized backscattering cross section with respect to $4\pi a^2$ as a function of frequency (ka) for different descriptive shapes and incident wave directions along O_z ($k=k_z$) and O_x ($k=k_r$).

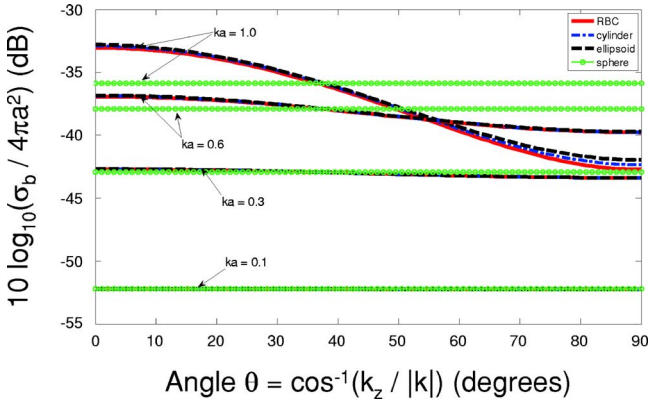

FIG. 5. (Color online) Angle dependency of the normalized backscattering cross section for different descriptive shapes at $ka=0.1$, 0.3, 0.6, and 1.0 (frequencies of 8.7, 26.1, 52.2, and 87 MHz). The angle θ is the angle between O_z and the incident wave direction.

D. Dependence of the backscattering cross section on the angle of incidence of the transmitted wave

At four frequencies corresponding to $ka=0.1$, 0.3, 0.6, and 1.0, the angular dependencies of BCS between 0° and 90° (angle between $\mathbf{e}_z$ and $\mathbf{k}$) are shown in Fig. 5 for the RBC, and the cylindrical, ellipsoidal, and spherical shapes. For the spherical particle, no angular dependencies are noted, as expected. At 8.7 MHz ($ka=0.1$), isotropic scattering is verified for all particles. Non-Rayleigh anisotropic scattering is observed at 26, 52, and 87 MHz for the RBC, cylinder, and ellipsoid. The angular variability of BCS increases for anisotropic particles as the frequency is increased. For example, variations of the order of 10 dB are noted at 87 MHz for the RBC.

IV. DISCUSSION

The backscattering cross section of weak scattering particles with arbitrary shapes can be semianalytically computed in the Born approximation. In this case, a Fourier duality exists between the geometry of the scatterer and the wave vector dependence of the backscattering cross section. A semianalytical model of the RBC profile enabled to compare the BCS of a red cell modeled by a biconcave volume with the BCS of simpler geometrical shapes. The notion of equivalence between two types of particles was defined in the low frequency scattering regime. Two particles with any given shape (sphere, ellipsoid, cylinder,…) were defined equivalent if the coefficients of the Taylor expansion of the BCS as a function of the wave number coincided up to the sixth order. Up to the sixth order, finding a shape equivalent to the RBC basically consists in matching first their volume and then their inertia axes as defined by the inertia tensor $\mathbf{\Sigma}$.

A. Weak scattering approximation

The computation of the BCS of fluid particles by Eq. (5) follows the first-order Born approximation: it is valid when the scattered wave amplitude remains negligible with respect to the incident wave. The case of scattering by a sphere that has the volume of a RBC is of interest to investigate the validity of this approximation.

TABLE III. Transition frequency (and of ka) above which biconcave RBC scattering differs by more than 5% than reference particle shapes.

	Rayleigh	Sphere	Second-order approximation of a RBC	Ellipsoid	Cylinder
ka	0.20	0.24	0.45	1.06	1.55
Frequency (MHz)	18	21	39	92	135

According to Refs. 9 and 17, Anderson's exact solution[18] of sphere backscattering and the Born approximation are in close agreement for frequencies corresponding to $0 \leqslant ka \leqslant 1$ (frequency $\leqslant$87 MHz). In the case of weak scatterers, the physical reasons for the nonvalidity of the Born approximation are the presence of multiple scattering, which is very unlikely for a single scatterer, and the arising of a resonance phenomenon. Minnaert resonance frequency for a fluid sphere predicts resonance for a wave number corresponding to $ka=3^{1/2}$ (i.e., a frequency of 150 MHz).

Even if the scatterer is not strictly spherical, multiple scattering is improbable due to the small contrasts in density and compressibility. Resonant frequencies are more difficult to predict, but one can postulate that it should occur around 150 MHz for a RBC. Therefore, for practical purpose, one can estimate that our BCS prediction must be valid up to ~87 MHz, whereas the predictions for frequencies higher than 87 MHz would have to be confronted to acoustical scattering simulations that take non-Born conditions into account.

B. Transition frequency to the non-Rayleigh scattering regime

The shape of a given particle influences the BCS through the nondimensional form factor $F(\mathbf{k})$. Under Rayleigh scattering conditions ($ka \ll 1$), the BCS is essentially independent on the particle shape, as $F(\mathbf{k}) \approx 1$. Increasing the frequency and changing the insonification angle enable to extract geometric details finer than the simple volume at the spatial scale of the wavelength. Having computed $F(\mathbf{k})$ for different descriptive shapes as a function of frequency and angle, one can assess the transition frequency to which their BCS differ by less than 5% of the Rayleigh limit $[F(\mathbf{k})=1]$. The bounds are given in Table III. For practical purpose, the biconcave RBC and the flat cylinder behave equivalently for frequencies below 90 MHz.

C. Comparison with previous studies

Using the T-matrix numerical method, Kuo and Shung[8] predicted that the shape (modeled by a sphere, a rounded cylinder and a realistic biconcave shape all having the same volumes) was of minor importance for frequencies below 30 MHz, and that the simulated BCS exhibited a k^4 dependence at those frequencies. However, their results at $ka < 0.1$ showed a dependence of the BCS with the angle of

incidence of the incident wave, and that the different types of BCS (cylinder, biconcave disk, sphere) had diverging values even when $ka \to 0$. This notably contradicts Rayleigh law that states that low frequency BCS from particles having the same volume and same acoustical properties do not differ and are moreover isotropic. One could attribute these discrepancies to the numerical T-matrix approach. For instance, low stability and approximation formulas of special functions can induce such errors. In our study, the angle and shape influences were negligible up to 21 MHz, and the RBC behaved as a sphere. We predict that angular variations from a single particle can only be observed above 21 MHz, if one considers that differences are significant when larger than 5%.

Coussios[9] also proposed an analytical approach to compute the scattering cross section of a RBC. The present study can be considered as a generalization of the previous formulation to a more realistic RBC shape, as it similarly used the Fourier integral formulation of the cross section. Our results are, however, restricted to the BCS (that considers $\mathbf{e}_r = -\mathbf{k}/k$) as the 180° scattering angle prevails in medical US. In Ref. 9, the RBC morphology was modeled by two types of isovolumic cylinders. By introducing the notion of acoustical inertia tensor, our study permits to find the dimensions of the equivalent cylinder by matching its inertia axes with the realistic RBC shape. Our conclusions concerning the bounds of the different scattering regimes are close to the predictions made by Coussios.[9] Moreover, our results readily showed that the biconcave RBC and the acoustical equivalent cylinder similarly backscatter ultrasonic waves, with a 5% accuracy for $ka < 1$ ($f < 87$ MHz).

D. A new approximation formula for the frequency dependence of backscattering from a scatterer with cellular dimensions

According to the second order approximation of the form factor of a RBC (using the acoustical inertia tensor) that predicts Rayleigh scattering up to 39 MHz ($ka = 0.44$), it seems appropriate to state that current medical US systems are not sensitive to geometric details of scatterers below the cell scale dimension of ~ 5 μm. Such details may only be detected if one considers higher frequencies. Accordingly, we can propose here a simple model of frequency dependence of the BCS of any type of weak scattering homogeneous particles with micrometric size:

$$\sigma_b(k\mathbf{e}_x) = \frac{1}{4\pi^2} k^4 V_s^2 \langle \gamma_z \rangle^2 (1 - 4\Sigma_{xx} k^2 + \cdots)$$

$$\approx \frac{1}{9} \langle \gamma_z \rangle^2 k^4 a^6 - \frac{4}{9} \Sigma_{xx} \langle \gamma_z \rangle^2 k^6 a^6. \quad (15)$$

In this expression, $\Sigma_{xx} = \mathbf{e}_x \Sigma \mathbf{e}_x$ is the component of the inertia tensor along the direction of propagation of the insonifying wave and a is the effective radius defined by $\frac{4}{3}\pi a^3 = V_s$. Notice that the resulting frequency dependence is here approximated by a sixth-order polynomial, with two nonvanishing coefficients. The coefficient in k^4 represents the Rayleigh contribution and the second coefficient in k^6 is the contribution of the inertia axis along O_x (the second order geometric correction is similar to the Guinier radius of gyration extracted from neutron/x-ray diffraction studies[19]).

E. Frequency dependence of backscattering from a collection of scatterers with cellular dimensions

Classical models of backscatter in US tissue characterization studies[5] usually model the frequency dependence by a power law:

$$\sigma_b(k\mathbf{e}_x) = \sigma_0 (k/k_0)^n, \quad (16)$$

where σ_0 is the low-frequency limit of the BCS, k_0 is a reference wave number (often selected at 1 MHz), and n is the spectral slope. This nonlinear regression is characterized by two material properties $\{\sigma_0, n\}$ in a given frequency range. According to our analytical study, an alternative set of frequency independent parameters $\{\langle \gamma_z \rangle V_s, \Sigma_{xx}\}$, derived from Eq. (15), would be more pertinent for US particle characterization. This new approach of data reduction should deserve some attention.

1. Characterization of RBC aggregation

The average number density of RBCs in blood is $m \approx 5 \times 10^6$ mm^{-3}, for a volume fraction $H = mV_s \approx 40\%$. Blood can be seen as a very dense suspension of red cells. As each RBC is surrounded by many neighboring cells, particle interactions are strong. The backscattering coefficient $\chi(\mathbf{k})$, or differential backscattering cross section from a collection of cells, defined as the BCS of the group of cells by unit volume, can be expressed as[20,21]

$$\chi(\mathbf{k}) = m\sigma_b(\mathbf{k}) S(-2\mathbf{k}), \quad (17)$$

where $S(-2\mathbf{k})$ is the structure factor and $\sigma_b(\mathbf{k})$ is the BCS of the individual RBC. The structure factor represents a corrective term taking into account the spatial correlations between scatterers. If RBCs independently scatter US, its value would simply be one. However, RBC mutual interactions induced by the strong particle number density and adhesion forces leading to cell clustering result in a strong deviation of $S(-2\mathbf{k})$ from one. The feasibility of measuring experimentally this deviation would rely on a good model of red cell BCS as:

$$S(-2\mathbf{k}) = \chi(\mathbf{k})/m\sigma_b(\mathbf{k}). \quad (18)$$

The backscattering coefficient $\chi(\mathbf{k})$ can be measured experimentally, m can be approximated by measuring the hematocrit in a microtube following centrifugation and the mean volume of RBCs, whereas $\sigma_b(\mathbf{k})$ can be approximated by Eq. (15). It is then straightforward to obtain the structure factor and its frequency dependence to characterize cell aggregation.

2. Potential use of US in hematology

The erythrocyte BCS may also be of interest for hematological profiling, as proposed in the late seventies.[22] Diluted suspensions of RBCs (at $H < 8\%$) roughly have a unit structure factor, which yields to $\chi(\mathbf{k}) = m\sigma_b(\mathbf{k})$. The measurements of the backscatter coefficient and of the hematocrit permit a straightforward derivation of the RBC volume V_s

and inertia axes from $\boldsymbol{\Sigma}$. A number of genetic diseases alter erythrocyte morphology and deformability (hereditary anemia as β-thalassemia, sickle cell anemia, spherocytosis, etc.). It could be of interest to develop such US tools that would allow a characterization of the related phenotypes, by studying the volume and shape response of pathologic RBCs to pH, pO_2, osmotic, or mechanical stimuli. Such studies may eventually be attempted *in vitro* or *in vivo* in the microcirculation where the volume fraction of RBCs is reduced.

V. CONCLUSION

A semianalytical expression of the erythrocyte ultrasonic backscattering cross section has been proposed. It took into account the acoustical contrasts between plasma and cell hemoglobin and the peculiar biconcave shape of the RBC. Provided the Born approximation is valid, the frequency and angle dependencies of the erythrocyte BCS were evaluated up to 90 MHz. By the use of these results as a reference, the accuracy of several other simplified analytical formulas could be assessed. The Rayleigh approximation (form factor=1, angle and shape independencies) appeared satisfactory up to 18 MHz; a quadratic correction of the form factor gave good approximations up to 39 MHz (over all insonifying angles, with errors below 5%). By deriving the inertia tensor $\boldsymbol{\Sigma}$ from the Hessian of the form factor $F(\mathbf{k})$ at a frequency of 0 Hz, the notion of acoustical inertia axis of a homogeneous scattering particle was defined. The RBC was shown acoustically equivalent to a thin cylinder of height 2 μm and diameter 7.8 μm or to an oblate spheroid of semi axes 4.3 and 1.2 μm ($f \leqslant 90$ MHz) as those simple shapes and the biconcave RBC have equivalent volume and acoustical inertia tensors. These findings give new bases to the description of the scattering of US by blood. The knowledge of the backscattering by a single erythrocyte is necessary to further study US scattering by millions of packed RBCs, as required to properly characterize red cell adhesion in shear flow.

ACKNOWLEDGMENTS

This work was supported by Grant No. MOP-36467 from the Canadian Institutes of Health Research. The second author is recipient of the National Scientist Award from the "Fonds de la Recherche en Santé du Québec" (2004–2009).

APPENDIX A

This appendix details the computations required to obtain the form factor of a symmetrical scatterer that has a relative impedance contrast given by $\gamma_z(\mathbf{r}) = \gamma_z(r,\theta,z) = \langle \gamma_z \rangle \mathbf{I}_{[|z|<z_0(r)]}$, where $z_0(r)$ is the radial profile of the scatterer shape, (r,θ,z) are the cylindrical coordinates, and $\langle \gamma_z \rangle$ is the homogeneous contrast of acoustical impedance of the particle.

The backscattering cross section of a scatterer in the Born approximation can be obtained from the general formulation of Eq. (3). That is given by

$$\sigma_b(\mathbf{k}) = \frac{k^4}{4\pi^2} \left| \int_{V_s} \gamma_z(\mathbf{r}) e^{2i\mathbf{k}\cdot\mathbf{r}} d^3r \right|^2. \tag{A1}$$

This integral can be written in a cylindrical system of coordinates, i.e.,

$$\sigma_b(\mathbf{k}) = \frac{k^4}{4\pi^2} \left| \int \gamma_z(r,\theta,z) e^{2i(k_r r \cos\theta + k_z z)} r dr d\theta dz \right|^2. \tag{A2}$$

The symmetries of the acoustical impedance allow to simplify Eq. (A2) to

$$\begin{aligned}\sigma_b(\mathbf{k}) &= \frac{k^4}{4\pi^2} \langle \gamma_z \rangle^2 \left| \int r \mathbf{I}_{[|z|<z_0(r)]} e^{2i(k_r r \cos\theta + k_z z)} dr d\theta dz \right|^2 \\ &= \frac{k^4}{4\pi^2} \langle \gamma_z \rangle^2 \left| \int r dr \int dz \mathbf{I}_{[|z|<z_0(r)]} e^{2ik_z z} \right. \\ &\quad \left. \times \int_{-\pi}^{\pi} d\theta e^{2ik_r r \cos\theta} \right|^2. \end{aligned} \tag{A3}$$

Now, the equality

$$J_0(x) = \frac{1}{2\pi} \int_{-\pi}^{\pi} e^{ix\cos\theta} d\theta \tag{A4}$$

is used to compute the integral in θ:

$$\sigma_b(\mathbf{k}) = k^4 \langle \gamma_z \rangle^2 \left| \int J_0(2k_r r) r dr \int \mathbf{I}_{[|z|<z_0(r)]} e^{2ik_z z} dz \right|^2. \tag{A5}$$

As

$$\int \mathbf{I}_{[|z|<x]} e^{2iuz} dz = 2x \,\mathrm{sinc}(2ux), \tag{A6}$$

where sinc represents the sinus cardinal function, then Eq. (A5) can be simplified to:

$$\sigma_b(\mathbf{k}) = 4k^4 \langle \gamma_z \rangle^2 \left| \int r J_0(2k_r r) z_0(r) \mathrm{sinc}(2k_z z_0(r)) dr \right|^2. \tag{A7}$$

As the form factor $F(\mathbf{k})$, given in Eq. (4), is defined by the formula:

$$\sigma_b(\mathbf{k}) = \frac{k^4 V_s^2}{4\pi^2} \langle \gamma_z \rangle^2 F(\mathbf{k}), \tag{A8}$$

then the comparison of Eq. (A7) with Eq. (A8) gives

$$F(\mathbf{k}) = \frac{16\pi^2}{V_s^2} \left| \int r J_0(2k_r r) z_0(r) \mathrm{sinc}(2k_z z_0(r)) dr \right|^2. \tag{A9}$$

To further simplify, let the volume of the scatterer be written as

$$V_s = \int r \mathbf{I}_{[|z|<z_0(r)]} dr d\theta dz = 4\pi \int z_0(r) r dr. \tag{A10}$$

This results in the following expression of the form factor:

$$F(k_r\mathbf{e}_r,k_z\mathbf{e}_z)=\left|\frac{\int rJ_0(2k_r r)z_0(r)\mathrm{sinc}(2k_z z_0(r))dr}{\int rz_0(r)dr}\right|^2. \quad \text{(A11)}$$

Finally, to obtain a normalized expression of $F(\mathbf{k})$, it can be recalled from Eq. (6) that $z_0(r)=h_0\phi(u)/2$, where $u=2r/D$. By rearranging Eq. (A11), the expected formula of the form factor given in Eq. (7) is obtained:

$$F(k_r\mathbf{e}_r,k_z\mathbf{e}_z)=\left|\frac{\int_0^1 u\phi(u)J_0(k_r Du)\mathrm{sinc}(k_z h_0\phi(u))du}{\int_0^1 u\phi(u)du}\right|^2. \quad \text{(A12)}$$

APPENDIX B

The second order expansion of the form factor of an homogeneous scatterer of volume V_s centered in O takes the form $F(\mathbf{k})=1-4\mathbf{k}\cdot\boldsymbol{\Sigma}\mathbf{k}+O(k^2a^2)$. This appendix proves that:

$$\boldsymbol{\Sigma}=\frac{1}{V_s}\int_{V_s}\mathbf{r}\otimes\mathbf{r}d^3r. \quad \text{(B1)}$$

Let's consider the Born approximation of the backscattering cross section, as given by Eq. (A1):

$$\sigma_b(\mathbf{k})=\frac{k^4}{4\pi^2}\left|\int_{V_s}\gamma_z(\mathbf{r})e^{2i\mathbf{k}\cdot\mathbf{r}}d^3r\right|^2. \quad \text{(B2)}$$

As $e^x=1+x+x^2/2+\cdots$, the second order expansion in $\mathbf{k}$ of Eq. (B2) is

$$\sigma_b(\mathbf{k})=\frac{k^4}{4\pi^2}\left|\int_{V_s}\gamma_z(r)(1+2i\mathbf{k}\cdot\mathbf{r}-2(\mathbf{k}\cdot\mathbf{r})^2+\cdots)d^3r\right|^2. \quad \text{(B3)}$$

By definition of the dyadic product,

$$(\mathbf{k}\cdot\mathbf{r})^2=\mathbf{k}(\mathbf{r}\otimes\mathbf{r})\mathbf{k}. \quad \text{(B4)}$$

As the scatterer is homogeneous and centered in O:

$$\int_{V_s}\gamma_z(\mathbf{r})\mathbf{r}d^3r=\langle\gamma_z\rangle\int_{V_s}\mathbf{r}d^3r=0. \quad \text{(B5)}$$

Consequently, combining Eqs. (B3)–(B5), and using $\gamma_z(\mathbf{r})=\langle\gamma_z\rangle\mathbf{I}_{[r\in V_s]}$, one obtains:

$$\sigma_b(\mathbf{k})=\frac{k^4}{4\pi^2}\langle\gamma_z\rangle^2\left|\int_{V_s}d^3r-2\mathbf{k}\cdot\left(\int_{V_s}\mathbf{r}\otimes\mathbf{r}d^3r\right)\mathbf{k}+\cdots\right|^2, \quad \text{(B6)}$$

or

$$\sigma_b(\mathbf{k})=\frac{k^4}{4\pi^2}\langle\gamma_z\rangle^2V_s^2\left(1-4\mathbf{k}\cdot\left(\frac{1}{V_s}\int_{V_s}\mathbf{r}\otimes\mathbf{r}d^3r\right)\mathbf{k}+\cdots\right). \quad \text{(B7)}$$

The comparison of Eq. (B7) to the definition of Eq. (4) of the form factor $F(\mathbf{k})$ yields the expected result:

$$F(\mathbf{k})=1-4\mathbf{k}\cdot\left(\frac{1}{V_s}\int_{V_s}\mathbf{r}\otimes\mathbf{r}d^3r\right)\mathbf{k}+\cdots. \quad \text{(B8)}$$

[1] M. F. Insana and D. G. Brown, "Acoustic scattering theory applied to soft biological tissues," in *Ultrasonic Scattering in Biological Tissues*, 1st ed., edited by K. K. Shung and G. A. Thieme (CRC Press, Boca Raton, FL, 1993), Chap. 4, pp. 75–124.

[2] F. L. Lizzi, M. Ostromogilsky, E. J. Feleppa, M. C. Rorke, and M. M. Yaremko, "Relationship of ultrasonic spectral parameters to features of tissue microstructure," IEEE Trans. Ultrason. Ferroelectr. Freq. Control **34**, 319–329 (1987).

[3] A. A. Aiazian, M. A. Taams, F. J. Ten Cate, and J. R. T. C. Roelandt, "Spontaneous echocontrast: Etiology, technology dependence and clinical implications," in *Advances in Echo Imaging Using Contrast Enhancement*, 2nd Ed., edited by N. C. Nanda, R. Schlief, and B. B. Goldberg (Kluwer Academic, Dordrecht, Boston, 1997), Chap. 4, pp. 65–83.

[4] I. W. Black, "Spontaneous echo contrast: where there's smoke there's fire (review)," Echocardiogr. **17**, 373–382 (2000).

[5] K. K. Shung and G. A. Thieme, *Ultrasonic Scattering in Biological Tissues*, 1st ed., edited by K. K. Shung and G. A. Thieme (CRC Press, Boca Raton, FL, 1993).

[6] A. Ishimaru, "Scattering and absorption of a wave by a single particle," in *Wave Propagation and Scattering in Random Media*, 1st ed., edited by A. Ishimaru (Academic, New York, 1978), Vols. **1** and **2**, pp. 9–27.

[7] T. K. Stanton, D. Chu, P. H. Wiebe, and C. S. Clay, "Average echoes from randomly oriented random-length finite cylinders: Zooplankton models," J. Acoust. Soc. Am. **94**, 3463–3472 (1993).

[8] I. Y. Kuo and K. K. Shung, "High frequency ultrasonic backscatter from erythrocyte suspension," IEEE Trans. Biomed. Eng. **41**, 29–34 (1994).

[9] C. C. Coussios, "The significance of shape and orientation in single-particle weak-scatterer models," J. Acoust. Soc. Am. **112**, 906–915 (2002).

[10] P. M. Morse and K. U. Ingard, "The scattering of sound," in *Theoretical Acoustics*, 1st ed., edited by P. M. Morse and K. U. Ingard (Mc-Graw-Hill, New York, 1968), Vol. **8**, pp. 400–446.

[11] D. Colton, J. Coyle, and P. Monk, "Recent developments in inverse acoustic scattering theory," SIAM Rev. **42**, 369–414 (2000).

[12] J. J. Bowman, T. B. A. Senior, and P. L. E. Uslenghi, *Electromagnetic and Acoustic Scattering by Simple Shapes* (North-Holland, Amsterdam, 1969).

[13] E. Evans and Y. C. Fung, "Improved measurements of the erythrocyte geometry," Microvasc. Res. **4**, 335–347 (1972).

[14] A. Rao, *Dynamics of Particles and Rigid Bodies* (Cambridge University Press, Cambridge, U.K., 2006).

[15] K. K. Shung, R. A. Sigelmann, and J. M. Reid, "Scattering of ultrasound by blood," IEEE Trans. Biomed. Eng. **23**(6), 460–467 (1976).

[16] C. C. Coussios, "Monitoring of hemolysis by acoustic scattering," Ph.D. Thesis, University of Cambridge, Cambridge, U.K., 2001.

[17] R. A. Roy, "Quantitative particle characterization by scattered ultrasound," Ph.D. Thesis, Yale University, 1987.

[18] V. C. Anderson, "Sound scattering from a fluid sphere," J. Acoust. Soc. Am. **22**, 426–431 (1950).

[19] A. Guinier and J. Fournet, *Small Angle Scattering of X-rays* (Wiley Interscience, New York, 1955).

[20] I. Fontaine, D. Savéry, and G. Cloutier, "Simulation of ultrasound backscattering by red cell aggregates: Effect of shear rate and anisotropy," Biophys. J. **82**, 1696–1710 (2002).

[21] D. Savéry and G. Cloutier, "A point process approach to assess the frequency dependence of ultrasound backscattering by aggregating red blood cells," J. Acoust. Soc. Am. **110**, 3252–3262 (2001).

[22] K. K. Shung and J. M. Reid, "Ultrasonic instrumentation for hematology," Ultrason. Imaging **1**, 280–294 (1979).